J Water Environ Nanotechnol 2026, 11(3): 326-344
10.22090/jwent.2025.2073827.1975

RESEARCH PAPER

Synthesis and Characterization of Peanut Shell-Derived Biochar-Nanobiochar Produced at 800 °C for Environmental Remediation

Deshraj Singh Thakur, Santosh Narayan Chadar*

Department of Chemistry, Govt. Autonomous Girls P.G. College of Excellence Sagar (M.P.); India

*Corresponding Author(s)
Email:
dr.santoshnarayan@gmail.com

Article History:
Received: 2025-10-06
Revised: 2025-12-15
Accepted: 2025-12-24

How to cite this article
Singh Thakur D and Narayan Chadar S. Synthesis and Characterization of Peanut Shell-Derived Biochar-Nanobiochar Produced at 800 °C for Environmental Remediation. J Water Environ Nanotechnol 2026, 11(3): 326-344, DOI: 10.22090/jwent.2025.2073827.1975

HIGHLIGHTS

- Peanut shell agricultural residue was valorized into biochar–nanobiochar through high-temperature slow pyrolysis, providing a potential route for converting biomass waste into a functional carbon material.
- Comprehensive characterization using SEM–EDX, FTIR, XRD, DLS–zeta potential, and BET revealed the morphological, chemical, structural, surface-charge, and textural properties of the synthesized material.
- Biochar–nanobiochar amendment demonstrated potential for improving soil chemical properties and nutrient availability, supporting its application as a sustainable soil-conditioning material.

ABSTRACT

The production of biochar from peanut shells via pyrolysis represents a sustainable strategy for converting agricultural residues into carbon-rich materials capable of improving soil quality. In this study, peanut shell biochar was prepared through slow pyrolysis at 800 °C for 3 h in a muffle furnace, and the influence of high-temperature carbonization on its physicochemical properties was systematically evaluated for soil amendment applications. The resulting biochar exhibited a BET surface area of 78.6 m^2/g, a total pore volume of 0.0708 cm^3/g, and an average pore diameter of 3.69 nm—features indicative of a predominantly mesoporous structure conducive to nutrient retention and water-holding capacity. Scanning electron microscopy revealed well-defined pore channels and a heterogeneous, rugged surface morphology, while Fourier-transform infrared spectroscopy showed diminished oxygenated functional groups and intensified aromatic C=C vibrations, reflecting substantial carbonization and enhanced structural stability. The elevated fixed carbon content and reduced volatile matter further corroborate the material's suitability for long-term carbon sequestration and soil conditioning. Overall, slow pyrolysis at 800 °C for 3 h yields peanut shell biochar with desirable surface characteristics, structural resilience, and mesoporosity, establishing its potential as an effective and sustainable soil amendment.

KEYWORDS:

Pyrolysis; Biochar; Nanobiochar; Soil fertility; Adsorption

©2026 The Author(s). Published by the Iranian Environmental Mutagen Society. This work is licensed under the Creative Commons Attribution 4.0 International License (CC BY 4.0). To view a copy of this license, visit http://creativecommons.org/licenses/by/4.0/.

1. INTRODUCTION

Soil constitutes a dynamic and multifunctional constituent of terrestrial ecosystems, exerting a pivotal influence on global biogeochemical cycles through the modulation of organic matter decomposition, nutrient cycling, and sustained carbon sequestration [1]. The maintenance of soil structure, aggregation, porosity, water-holding capacity, nutrient buffering, and biological activity depends heavily on soil organic carbon, which makes up about half of all soil organic matter [2,3]. As a result, sustaining soil organic carbon stores is essential for enhancing climate resilience, maintaining ecological stability, and ensuring global food security. However, SOC depletion is continuously accelerated by intensive land management techniques, soil erosion, and excessive chemical input use, which turns soils from carbon sinks to sources and increases greenhouse gas emissions into space [4,5].

The value of agricultural leftovers as stable, useful soil additions has increased due to these mounting environmental concerns. Agricultural byproducts rich in lignocellulosic compounds, primarily cellulose, hemicellulose, and lignin, have great potential for thermochemical conversion into environmentally friendly materials [6,7]. It is commonly known that soil management techniques like mulching, composting, adding biochar, and adding organic amendments can increase soil organic carbon stocks, improve soil fertility, and lessen the negative environmental effects of conventional fertilizers. These benefits are amplified by new nanoscale soil supplements, such as nanobiochar, nano-zeolites, and tailored nanoparticles, which have improved reactivity, improved nutrient retention, and increased effectiveness in soil remediation and pollutant sequestration [8-12].

Biochar, which is created by pyrolyzing organic feedstocks in oxygen-limited settings, has attracted a lot of scholarly attention due to its refractory aromatic carbon structure, rich surface functionalities, and porous architecture. These features enhance soil health overall and lessen the need for chemical fertilizers by encouraging better soil aeration, water retention, cation exchange capacity, and microbial habitat expansion [13,14]. When biochar is scaled to the nanoscale, it exhibits significantly improved physicochemical characteristics—such as increased surface area, better pore accessibility, and higher adsorption capacity—making nanobiochar incredibly effective for nutrient cycling, pollutant immobilization, and environmental remediation. The superior effectiveness of nano-enabled carbon materials in sorption, catalysis, phytoremediation enhancement, and pollution removal from soil-water systems has been demonstrated in numerous investigations [15-18].

Peanut shells are produced in significant amounts from the world's peanut output, making them a plentiful but underutilized lignocellulosic biomass. Over 53 million tons of peanuts are produced annually, with India being one of the main producers. As a result, agricultural waste streams are greatly increased [19]. This biomass, which accounts for approximately 30% of the peanut's overall mass, generates an estimated 11 million tonnes of waste annually. They are resistant to natural breakdown because of their strong lignocellulosic structure, which is mostly made up of cellulose, hemicellulose, and lignin. However, they are highly appropriate for conversion into stable, carbon-rich compounds like biochar. The effectiveness of nanobiochar made from peanut shells as an excellent material for soil amelioration, pollution remediation, and environmental engineering applications has been highlighted by recent academic studies [20-22].

The pyrolysis parameters, such as temperature, heating rate, retention time, and air environment, significantly influence the physicochemical characteristics of biochar, including its pore architecture, surface functional groups, elemental composition, and aromatic recalcitrance [23-25]. When pyrolysis is carried out at lower temperatures, more charcoal is usually produced while more oxygenated functional groups are retained. On the other hand, higher temperatures promote stronger aromatic condensation, increased thermal stability, increased porosity, and better surface reactivity, but at the expense of lower yields overall [26-28]. Peanut shells have been converted using a variety of pyrolysis techniques, including fixed-bed reactors, microwave-assisted pyrolysis, and muffle furnace treatments [29-31]. However, there are still a few thorough studies on the high-temperature synthesis of nanobiochar from peanut shells, together with thorough physicochemical characterization and evaluation of its effectiveness in improving soil. It is critical to close this research gap to improve carbon-based supplements for sustainable soil management and waste valorization techniques.

2. MATERIALS AND METHODS

2.1. Material Sourcing and Preparation

Peanut shells, the primary feedstock for this study, were sourced from agricultural sites in the Sagar district of Madhya Pradesh, India, an area recognized for its extensive groundnut farming. Following procurement, the shells underwent a meticulous cleaning process to remove soil, dust, and other contaminants. To prevent microbial degradation and preserve their intrinsic properties, the cleaned shells were air-dried and subsequently stored in shaded, well-ventilated conditions until use in biochar production [32,33].

2.2. Biochar-Nanobiochar Production

Biochar was produced by thermochemically pyrolyzing peanut shells in a stainless-steel tube reactor inside a muffle furnace. The biomass feedstock was pyrolyzed in a sealed tube with minimal oxygen for three hours at 800 °C in accordance

with standard protocols [34]. The resulting biochar was collected, weighed, and kept in sealed containers to avoid contamination and moisture adsorption once it had cooled to room temperature. The coarse biochar was then manually crushed with an agate mortar and pestle for three hours under ambient conditions before being filtered through a 200-mesh stainless-steel screen. The fraction that passed through the sieve was called peanut shell biochar [35]. Since the material's particle dimensions have a significant impact on its reactivity, dispersibility, specific surface area, and interactions with the environment, particle size comminution is a crucial procedure. The following formula was used to calculate the biochar yield:

$$\text{Biochar Yield}(\%) = \frac{\text{Weight of Biochar Obtained}}{\text{Weight of Feedstock Used}} \times 100$$

(Figure 1) Schematically represents the thermochemical conversion of peanut shells into biochar, a process executed within a muffle furnace.

2.3. Biochar-Nanobiochar Characterization

The biochar samples, produced at 800 °C for 3 hours within a muffle furnace, underwent comprehensive physicochemical characterization to ascertain their suitability for various soil and environmental applications. Organic carbon content was quantified using the Walkley–Black wet oxidation method [36]. Total nitrogen and phosphorus were analyzed in accordance with established procedures, while potassium determination followed recognized methodologies [37]. These characterizations yielded crucial information regarding the nutrient composition and prospective agricultural utility of the high-temperature biochar [38].

Chemical Analysis

The biochar, produced at 800 °C during a 3-hour pyrolysis, underwent comprehensive chemical characterization. Organic carbon content was ascertained through the Walkley–Black wet oxidation method. Total nitrogen, available phosphorus, and potassium were quantified using standard analytical procedures applicable to soil and biochar. Furthermore, sulphur, boron, and essential micronutrients—such as zinc, iron, copper, magnesium, sodium, calcium, and manganese—were precisely determined via Atomic Absorption Spectroscopy, flame photometry, and titrimetric methods, thereby ensuring analytical rigor and consistency [39].

Scanning Electron Microscopy (SEM–EDX)

Surface morphology and elemental composition were investigated using Scanning Electron Microscopy coupled with Energy Dispersive X-ray Spectroscopy. The analysis of pore structure and microstructural variations was facilitated by the system, which operated with T Microscope Control V6.2.8 software. Concurrently, elemental verification was performed via EDX analysis [40].

Fourier Transform Infrared Spectroscopy (FTIR)

Fourier Transform Infrared Spectroscopy was employed to characterize the functional groups and surface chemistry of the biochar, utilizing the KBr pellet method. This involved

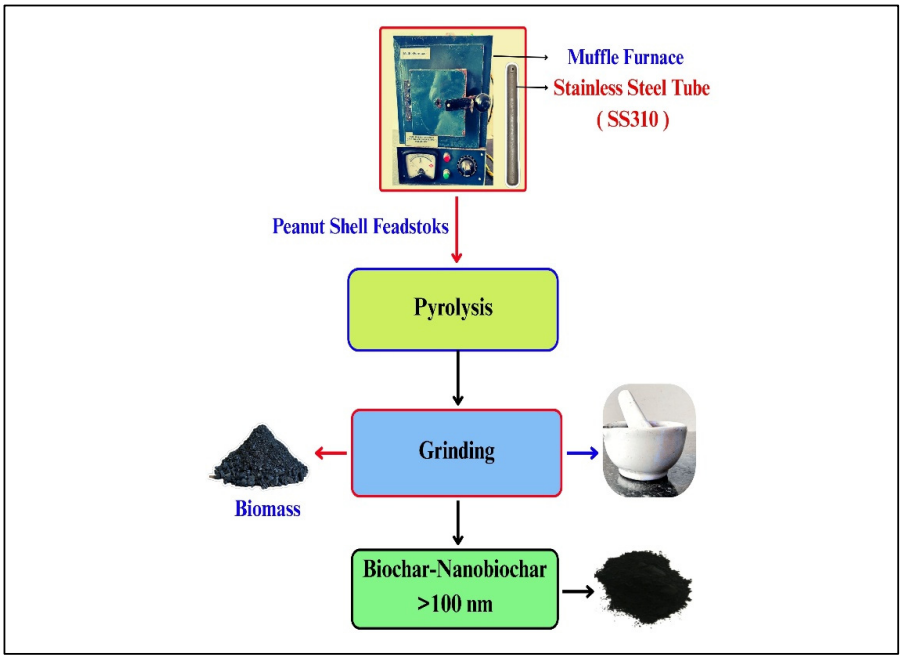

Fig. 1. Schematic representation of the preparation process of biochar from peanut shells through pyrolysis and grinding.

J Water Environ Nanotechnol, 2026, 11(3): 326-344
10.22090/jwent.2025.2073827.1975

grinding the biochar finely, mixing it with spectroscopic-grade potassium bromide, and compressing the mixture into pellets under vacuum. Spectra were acquired over a range of 4000–400 cm^{-1} at a resolution of 4 cm^{-1}, with 50 scans per sample to optimize signal accuracy. The resulting FTIR spectra presented distinct absorption peaks indicative of various functional groups: a broad band around 3400 cm^{-1} signified –OH stretching vibrations; peaks between 2920–2850 cm^{-1} were ascribed to aliphatic C–H stretching; a sharp band at approximately 1700 cm^{-1} pointed to C=O stretching of carboxylic and carbonyl groups; and peaks near 1600 cm^{-1} corresponded to aromatic C=C stretching. Furthermore, bands observed in the 1100–1000 cm^{-1} region suggested the presence of C–O–C and Si–O vibrations, indicating oxygenated and siliceous structures on the biochar surface. These identified functional groups are pivotal for adsorption and ion-exchange processes, thereby affirming the active surface chemistry of the 800 °C biochar. The analytical methodology and subsequent interpretation were conducted in accordance with established procedures [41].

X-ray Diffraction (XRD)

The crystalline structure and phase composition of the peanut shell biochar were analyzed using an X-ray Diffractometer, operating in the 2θ range of 10–80°. The resulting XRD pattern displayed broad and diffuse peaks, indicative of a predominant amorphous carbon structure with some degree of graphitization at 800 °C. Additionally, minor crystalline peaks corresponding to silica, potassium carbonate, and calcium oxide were identified, suggesting the presence of thermally stable inorganic minerals formed during the pyrolysis process. These findings confirm that high-temperature treatment promotes carbon ordering while preserving the inherent mineral residues of the peanut shell [42].

Biochar-Nanobiochar Stability Analysis

The stability of biochar was evaluated by chemical oxidation using a 5% H_2O_2 solution. Solution, adhering to the Edinburgh Biochar Stability Tool protocol. Carbon contents in samples were measured before and after oxidation with a Carbon/Nitrogen Analyzer employing the Dumas dry combustion method. This method facilitated differentiation between the labile carbon fraction vulnerable to oxidative breakdown and the recalcitrant, thermally persistent carbon in the biochar [43].

The stability percentage was calculated as:

$$\text{Stable C}\,(\%) = \frac{(\text{Carbon after } H_2O_2 \text{ treatment})}{(\text{Carbon before treatment})} \times 100$$

Soil Analysis

The impact of nanobiochar incorporation on soil physicochemical properties was evaluated at regular intervals. Soil pH and electrical conductivity were measured in a 1:2.5 soil-to-water suspension using a digital pH and conductivity meter. Organic matter content was determined by the Walkley–Black wet oxidation method. Available nitrogen was analyzed by the alkaline permanganate method, available phosphorus using the Olsen method, and exchangeable potassium through flame photometry after extraction with neutral normal ammonium acetate. Micronutrients such as iron, zinc, copper, and manganese were extracted using DTPA solution and quantified using Atomic Absorption Spectroscopy. These analyses were conducted to assess nutrient dynamics, soil fertility enhancement, and the agronomic efficiency of peanut shell-derived nanobiochar [44].

2.4. Statistical Analysis

Microsoft Excel was used to analyze all experimental data in order to maintain accuracy, consistency, and openness in data management. BET surface area, elemental composition, pH, electrical conductivity, soil nutrient tests, and adsorption parameters were among the analytical measurements that were repeated in triplicate (n = 3). Excel's built-in statistical functions were used to calculate the mean, standard deviation, coefficient of variation, and standard error of the mean for the resulting datasets.

3. RESULTS AND DISCUSSION

3.1. Biochar Yield under High-Temperature Pyrolysis

Biochar was synthesized from peanut shells using a muffle furnace operated at 800 °C for 3 hours under limited oxygen conditions. The yield was calculated as the ratio of the weight of biochar obtained to the initial weight of peanut shells. Increasing the pyrolysis temperature led to a noticeable reduction in biochar yield due to enhanced thermal degradation of lignocellulosic components such as cellulose, hemicellulose, and lignin. In this study, the biochar yield at 800 °C was lower than that typically obtained at moderate temperatures (450–600 °C), consistent with previous observations that yield decreases sharply with rising temperature. The decline in yield at higher temperatures is mainly due to volatilization of organic matter and the release of non-condensable gases during carbonization. Although high-temperature pyrolysis enhances the aromaticity, stability, and surface area of biochar, it results in a lower overall mass yield compared with low-temperature, slow-pyrolysis processes [45].

3.2. Chemical Composition of Biochar

The high pyrolysis temperatures used in this work had a significant impact on the chemical makeup of peanut shell biochar. The Walkley-Black method revealed a significantly reduced oxidizable organic carbon content in biochar produced by pyrolysis at 800 °C. This decrease is caused by the assay's incapacity to oxidize the highly aromatic and condensed carbon structures produced at high temperatures, rather than decreased

total carbon. Intense carbon condensation and aromatization are driven by pyrolysis at 800 °C, increasing fixed and total carbon proportions despite the reduced oxidizable fraction.

The nutritional profile of the biochar also reflected the effects of carbonization at high temperatures. Volatilization or thermal breakdown significantly reduced the amounts of nitrogen, phosphorus, calcium, and magnesium, while potassium was relatively concentrated because of its poor volatility and retention in the ash. During pyrolysis, micronutrients such as iron, zinc, manganese, copper, sodium, and boron were kept at measurable amounts, indicating partial mineral preservation.

Overall, these results show that high-temperature pyrolysis reduces oxidizable carbon and certain plant-accessible nutrients while increasing the biochar's structural stability, aromaticity, and fixed carbon content. Consequently, 800 °C biochar is more effective for long-term carbon sequestration than it is for short-term nitrogen replenishment [46].

3.3. Surface Morphology (SEM)

The microstructural analysis of peanut shell-derived biochar, conducted using scanning electron microscopy, revealed a highly diverse morphology, with particle dimensions spanning from sub-micron to roughly 5 µm. The observed particles displayed irregular, angular, and flaky characteristics, distinguished by rough, porous surface topographies that substantially augment the accessible surface area for adsorption and interaction with both soil nutrients and contaminants. Interspersed among larger plate-like formations were smaller granular fragments, suggesting the impact of mechanical and thermal breakdown processes during the biochar's synthesis. This combination of a porous texture and fragmented morphology collectively facilitates improved diffusion pathways and an increased number of reactive surface sites. Consequently, this positions the biochar as a highly efficient material for diverse environmental applications, including soil amelioration, pollutant sequestration, and water treatment. Collectively, these morphological attributes highlight the significant impact of pyrolysis conditions on biochar architecture and emphasize the promise of peanut shell-derived biochar as an economical and sustainable resource for enhancing soil fertility and mitigating environmental concerns.

3.4. Fourier transform infrared spectroscopy (FTIR)

The FTIR spectrum of biochar derived from peanut shells

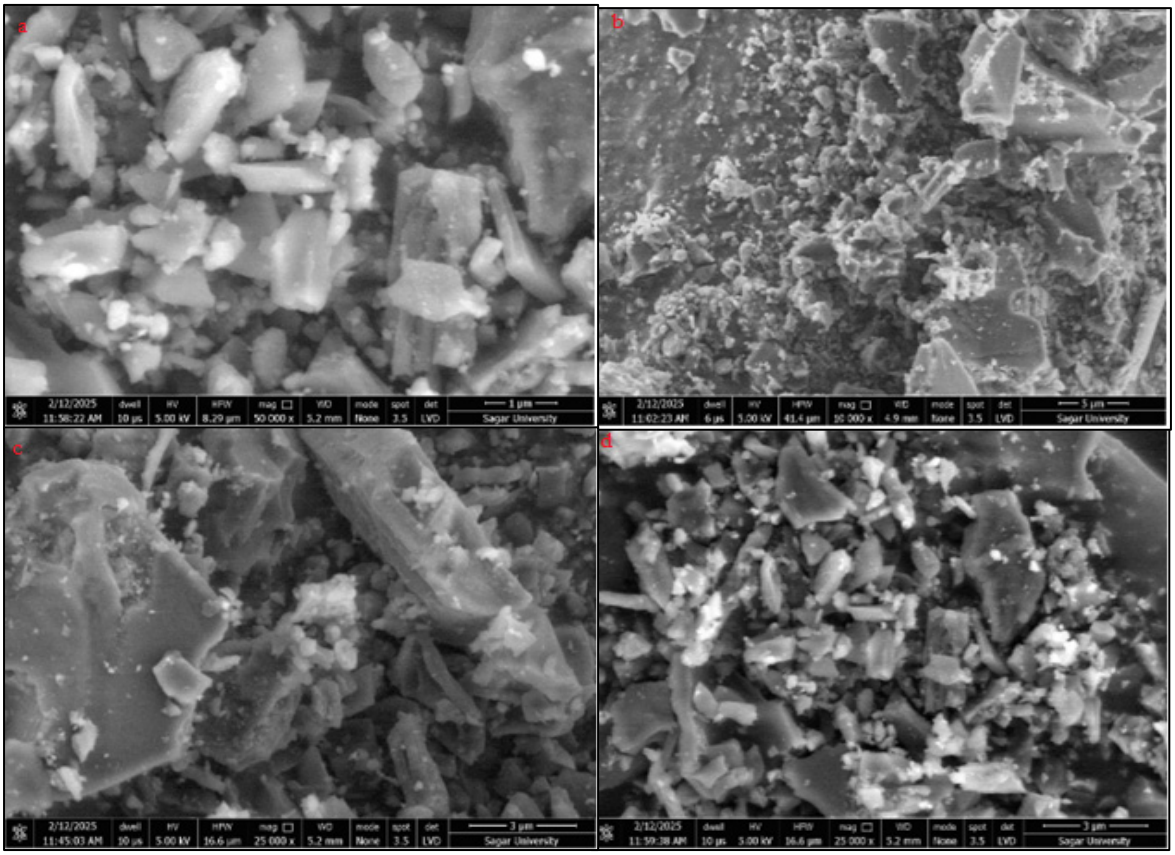

Fig. 2. SEM images (a–d) of peanut shell–derived biochar at different magnifications showing irregular, porous, and heterogeneous surface morphology.

J Water Environ Nanotechnol, 2026, 11(3): 326-344
10.22090/jwent.2025.2073827.1975

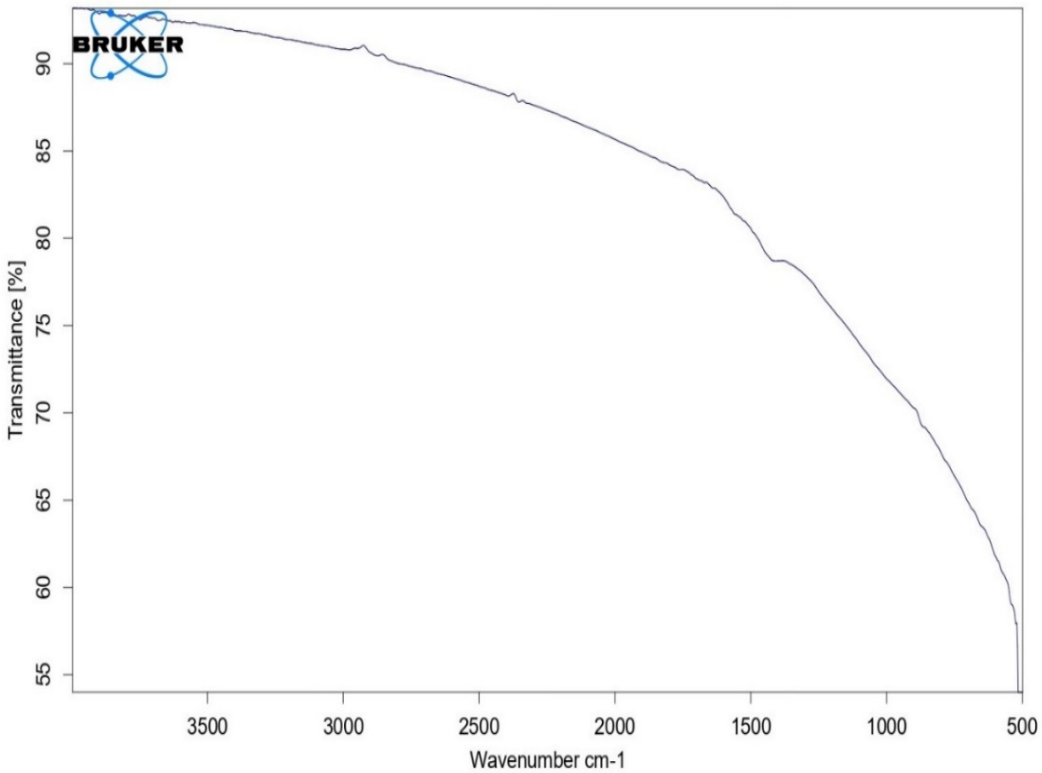

Fig. 3. FTIR spectrum of peanut shell–derived biochar showing major functional groups.

further substantiates this observation, displaying a broad decrease in transmittance with increasing wavenumber, characteristic of a blend of oxygenated and aromatic structures. A broad absorption band ranging from 3400–3200 cm^{-1} corresponds to O–H stretching vibrations of hydroxyl groups, denoting the presence of alcohols, phenols, and adsorbed moisture. Peaks around 2920–2850 cm^{-1} are associated with aliphatic C–H stretching, while the band between 1700 and 1600 cm^{-1} is attributed to C=O and aromatic C=C stretching, indicating partial oxidation and aromatic condensation. Absorptions in the 1400–1000 cm^{-1} range represent C–O stretching, typical of esters, ethers, and alcohols, whereas the region below 800 cm^{-1} suggests aromatic C–H out-of-plane bending vibrations, confirming the development of condensed aromatic rings. The presence of these functional groups significantly enhances the biochar's adsorption capacity, surface reactivity, and potential for environmental applications, such as pollutant removal and nutrient retention in soil systems.

3.5. X-ray Diffraction (XRD)

The XRD pattern of peanut shell biochar displays a mix of broad and sharp reflections, suggesting the presence of crystalline mineral phases and an amorphous carbon matrix. Disordered carbon produced during biomass pyrolysis is characterized by the wide hump seen between 20 and 30° (2θ). Inorganic mineral components like silica (SiO_2), calcite ($CaCO_3$), and metal oxides inherited from the peanut shell feedstock are represented by distinct diffraction peaks at 22.93°, 26.56°, 29.33°, 33.07°, 35.90°, 39.35°, 43.15°, 47.37°, 48.45°, 57.24°. The graphitic (002) plane is frequently associated with the reflection near 26.56° (2θ); however, complete graphitization is rarely achieved in biochars produced at 800 °C under non-catalytic conditions. Consequently, turbostratic carbon, which represents partially ordered aromatic carbon layers with random stacking and low long-range crystallinity, provides a better explanation for this peak. This interpretation is supported by the reflection's diffuse and wide scope. The semi-crystalline structure revealed by the XRD results consists of crystalline mineral inclusions embedded in a primarily disordered, turbostratic carbon framework. This structure helps to maintain the thermal stability of the biochar and offers heterogeneous surface sites that are advantageous for adsorption and soil conditioning applications.

3.6. Energy Dispersive X-ray (EDX)

Energy-dispersive X-ray spectroscopy analysis confirmed carbon as the primary constituent in peanut shell biochar, followed by oxygen, nitrogen, potassium, magnesium, and calcium. A slight increase in relative carbon content was observed under slow pyrolysis at 800°C, indicative of enhanced carbonization. Concurrently, oxygen and mineral elements

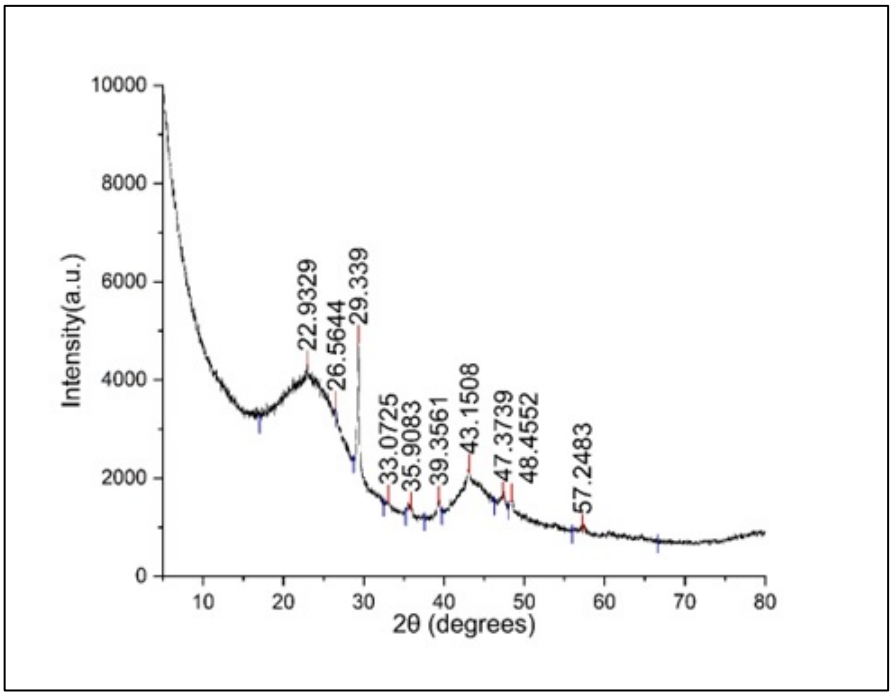

Fig. 4. XRD Pattern of Peanut Shell Biochar

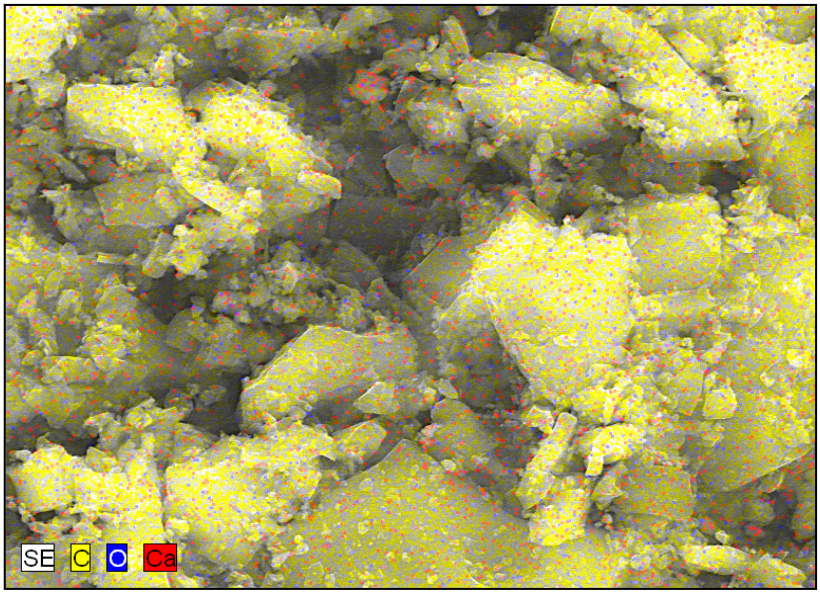

Fig. 5. EDS elemental mapping of peanut shell–derived biochar showing the distribution of C, O, and Ca.

like K and Mg showed higher concentrations at 800°C, reflecting partial oxidation and mineral enrichment at elevated temperatures. EDS elemental mapping of peanut shell-derived biochar additionally elucidated the spatial distribution of key elements, including carbon, oxygen, and calcium, across the biochar surface. The prevalence of yellow zones, correlating to carbon, underscored the highly carbonaceous nature of the biochar originating from lignocellulosic biomass. Uniformly dispersed blue regions, representing oxygen, signaled the presence of oxygen-containing functional groups such as hydroxyl, carbonyl, and carboxyl, which augment surface reactivity and adsorption capacity. Red spots, corresponding to calcium, were distributed across the surface, signifying the integration of inorganic mineral phases, either intrinsic to the

J Water Environ Nanotechnol, 2026, 11(3): 326-344
10.22090/jwent.2025.2073827.1975

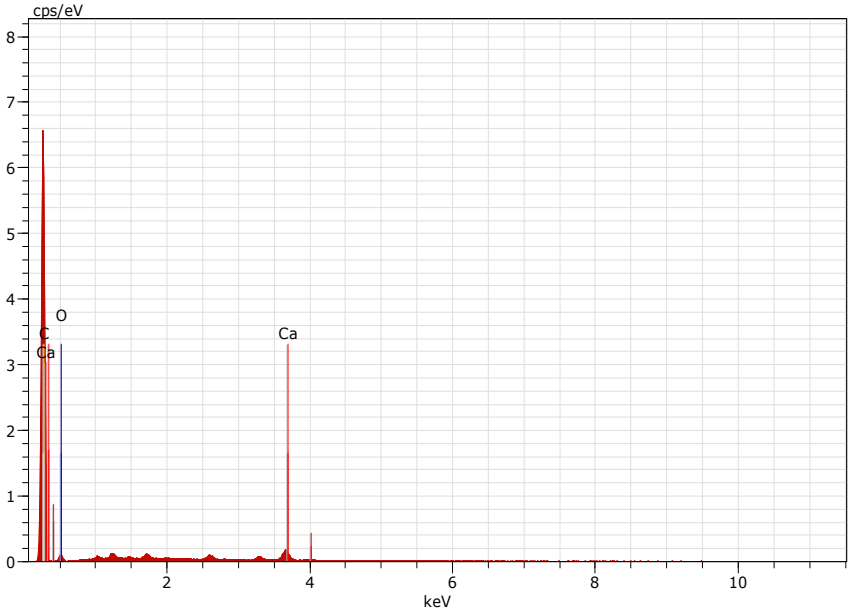

Fig. 6. EDS spectrum of the sample showing characteristic peaks of Carbon (C), Oxygen (O), and Calcium (Ca).

Table 1. Elemental composition of peanut shell–derived biochar obtained from EDX analysis.

Element	Atomic Number (Z)	Series	Normalized wt.%	Normalized at. %	Error (1 Sigma wt.%)
C	6	K-series	87.89	91.96	10.26
O	8	K-series	8.98	7.05	2.06
Ca	20	K-series	3.13	0.98	0.13
Total	—	—	100.00	100.00	—

biomass or formed during pyrolysis. The simultaneous presence of carbon, oxygen, and calcium highlights the biochar's heterogeneous composition, characterized by an organic carbon matrix enriched with inorganic mineral components. This composite structure collectively improves its efficacy in heavy metal adsorption, nutrient retention, and supporting environmental remediation processes.

The elemental composition of the peanut shell-derived biochar was definitively established by the Energy Dispersive X-ray Spectroscopy spectrum, which displayed distinct characteristic peaks. Signals indicative of carbon and oxygen were prominently observed in the low-energy

range, corresponding to the organic carbon matrix and oxygen-bearing functional groups commonly identified in biochar materials. Furthermore, a sharp and intense peak at approximately 3.7 keV confirmed the presence of calcium, suggesting the integration of mineral phases or inorganic residues either from the raw biomass or formed during high-temperature pyrolysis. The relative intensities of these detected peaks imply that the biochar is primarily carbon-rich, possessing surface oxygen functionalities, with calcium acting as a substantial inorganic component. This calcium content is presumed to augment the material's structural integrity, stability, and surface reactivity. The representative elemental composition of the sample, as derived from the EDS spectrum, is presented in Table 1.

3.7. Zeta Potential (Mobility and Particle Size Analysis)

The particle size analysis shows a clear contrast between the intensity and volume distributions, indicating a highly polydisperse system dominated by large agglomerates. In the intensity distribution, several peaks appear across the nano- to micro-scale range, demonstrating the presence of multiple particle populations. The large peak at the higher diameter region reflects strong light scattering by big aggregates, which dominate intensity-based measurements even if present in lower numbers. In comparison, the volume distribution exhibits a single prominent peak concentrated in the higher size range, indicating that the majority of the particle volume is contributed by these large aggregates, while smaller particles

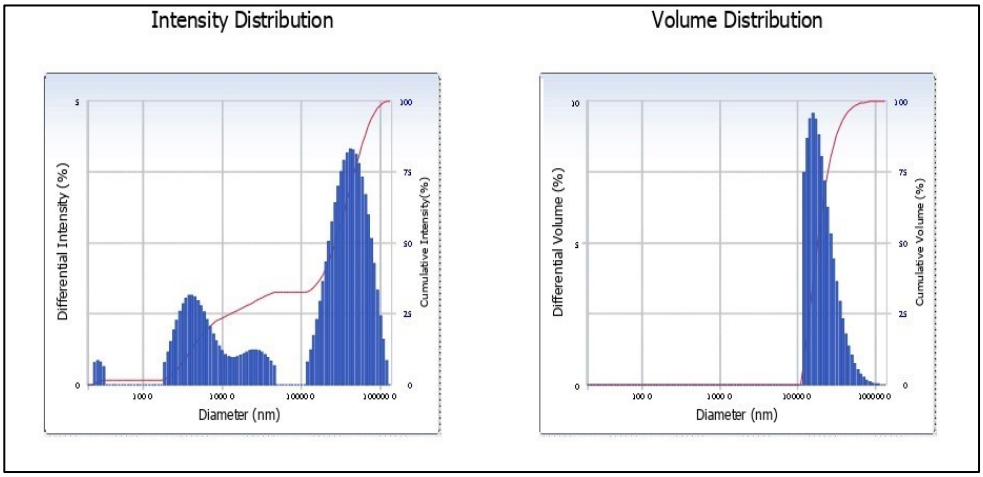

Fig. 7. Intensity and volume particle size distributions of the biochar, illustrating differences in particle population and cumulative percentage across measured diameters.

Table 2. Dynamic Light Scattering (DLS) measurement parameters of peanut shell–derived biochar.

Parameter	Value Unit	Notes
Temperature	25.1°C	Measurement condition
Diameter (d)	3169.0 nm	Hydrodynamic diameter
Diluent Name	WATER	Solvent used
Polydispersity Index (P.I.)	1.510	Distribution width
Refractive Index	1.3328	Optical property
Diffusion Constant (D)	1.556e-009 cm^2/sec	Molecular diffusion
Viscosity	0.8858 cP	Fluid property
Scattering Intensity	9936 cps	Photon count rate
Residual	7.870e-003	Fitting residual
Attenuator 1	52.64%	Instrument setting

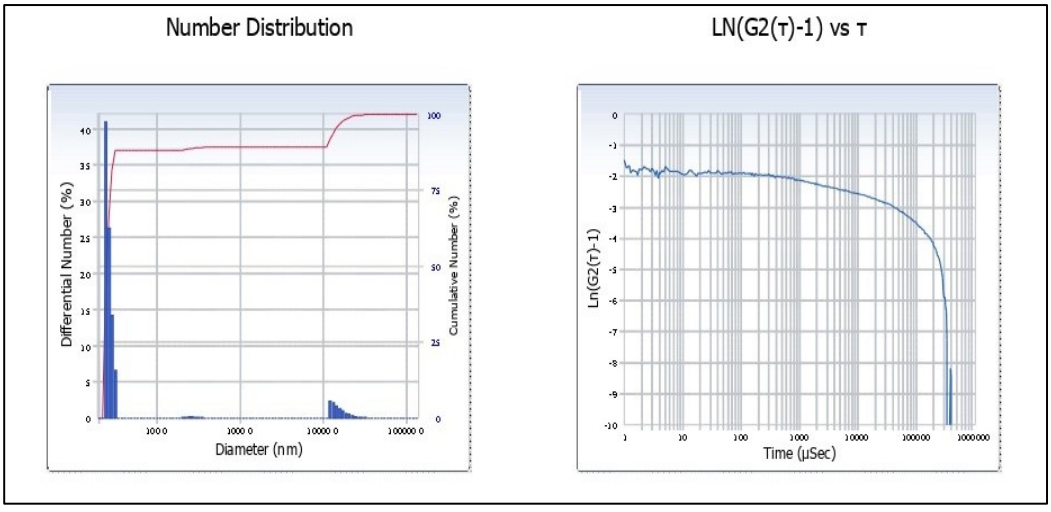

Fig. 8. Number-based particle size distribution and corresponding LN(G2(τ)−1) decay curve of the biochar sample.

J Water Environ Nanotechnol, 2026, 11(3): 326-344
10.22090/jwent.2025.2073827.1975

Table 3. Particle size distribution data of peanut shell–derived biochar obtained from DLS analysis.

Peak	Intensity Distribution Diameter (nm)	Std. Dev.	Volume Distribution Diameter (nm)	Std. Dev.	Number Distribution Diameter (nm)	Std. Dev.
1	27.3	2.6	26.5	2.5	25.9	2.3
2	529.0	274.7	341.4	120.7	278.2	63.7
3	2,721.3	915.2	2,314.6	635.8	1,975.3	416.1
4	48,429.2	24,707.1	23,200.1	11,291.2	16,420.1	4,669.9
5	0.0	0.0	—	—	—	—
Average	33,015.4	30,097.2	23,200.0	11,291.3	1,789.7	5,300.9

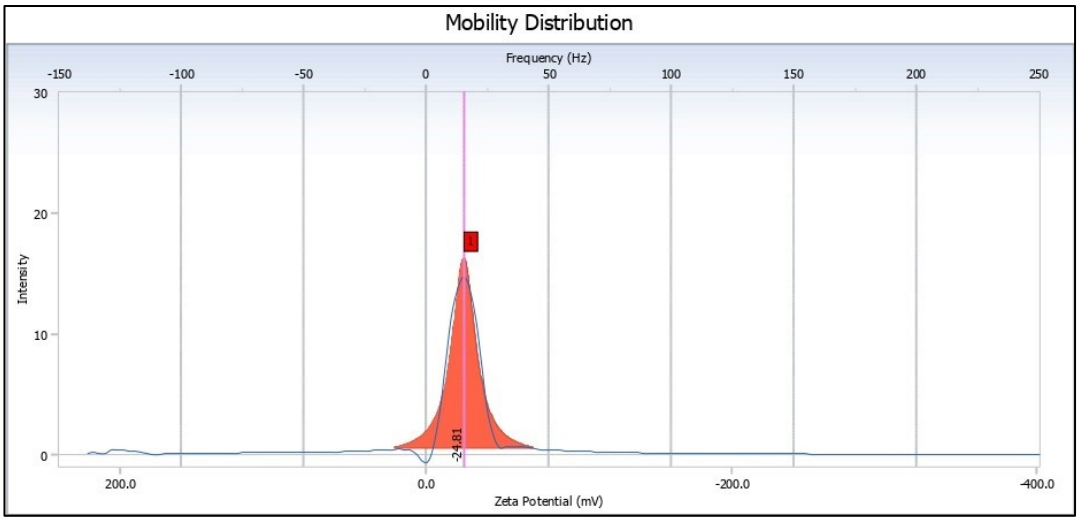

Fig. 9. Mobility distribution plot showing the zeta-potential peak of the biochar suspension, illustrating particle mobility and surface charge behavior.

Table 4. Zeta potential and electrophoretic mobility characteristics of peanut shell–derived biochar.

Parameter	Value	Notes / Grouping
Zeta Potential	-24.81 mV	Main measurement
Doppler Shift	15.46 Hz	Frequency shift
Mobility	-1.938e-004 cm^2/Vs	Particle movement
Base Frequency	124.6	Instrument setting
Conductivity	0.1299 mS/cm	Fluid property
Conversion Equation	Smoluchowski	Method used

contribute minimally to the overall volume. Together, these patterns confirm that the sample contains mixed particle sizes with significant aggregation, leading to a predominance of larger particles in the material.

The number-based particle size distribution shows that the majority of particles fall within the lower nanometer range, as indicated by the sharp, dominant peak at small diameters. This suggests that a large population of primary nanoparticles is present despite the significant agglomeration observed in the intensity and volume distributions. The minor peaks observed at higher diameters correspond to a small fraction of large aggregates, which contribute negligibly to the number fraction but strongly influence intensity-based measurements. The correlation function plot ($Ln(G_2(\tau)-1)$ vs τ) exhibits a gradual decay followed by a sharp decline at longer delay times, indicating the coexistence of fast- and slow-diffusing species. The initial rapid decay corresponds to the small, highly mobile nanoparticles, while the extended tail reflects the presence of

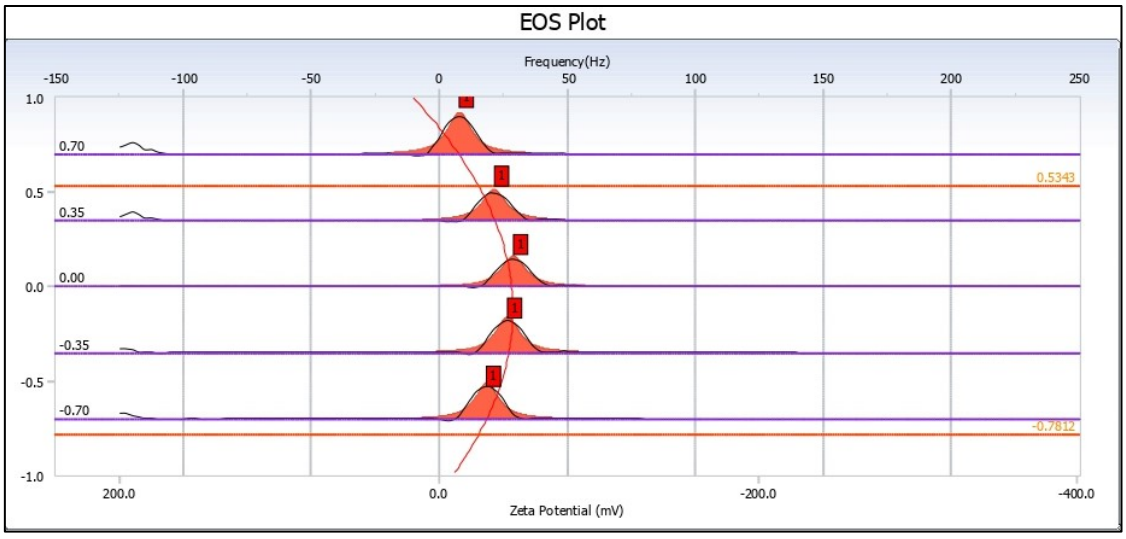

Fig. 10. EOS plot showing the zeta-potential distribution of the biochar sample at different applied frequencies. The red peaks represent the phase-shift response used to estimate surface charge behavior.

larger aggregates with slower Brownian motion. Together, these results confirm a polydisperse system composed of abundant nanoscale particles and a smaller proportion of micron-sized agglomerates, consistent with the multi-modal behavior typically observed in DLS analysis of carbonaceous or biochar-derived nanomaterials.

The mobility distribution reveals a single dominant peak centered at approximately −24.81 mV, indicating that the particles possess a moderately negative surface charge under the measurement conditions. The narrow and symmetrical shape of the peak suggests that the colloidal suspension contains one major electrophoretic population, with minimal contributions from secondary or broad mobility modes. This unimodal distribution implies that the surface functional groups of the particles are relatively uniform, which is consistent with a stable dispersion dominated by similarly charged particles. Although the magnitude of the zeta potential lies within the moderate stability range (−20 to −30 mV), it is sufficient to provide electrostatic repulsion that limits extensive aggregation, explaining the presence of discrete, smaller particles observed in the number distribution. The absence of significant side peaks or broad mobility tails further confirms that no major fraction of oppositely charged or weakly charged aggregates is present in the suspension. Overall, the zeta-potential profile supports that the sample maintains moderate colloidal stability, governed primarily by negatively charged surface functionalities.

The EOS plot presents the phase-resolved electrophoretic mobility response of the sample across a series of applied frequencies, revealing a consistent and well-defined peak in each scan. Across all positions (from +0.70 to −0.70), the zeta-potential distributions remain centered near the same mobility region, indicating that the electrophoretic behavior of the particles is homogeneous throughout the cuvette. The narrow, symmetric peaks in each layer demonstrate that the system contains a single dominant colloidal population with minimal contributions from secondary modes or oppositely charged species. The slight variations in peak height and width among the layers are expected from spatial changes in field strength during the phase analysis, but do not indicate any significant heterogeneity in surface charge. The signals observed on the extreme positive and negative sides correspond to low-intensity background noise and do not reflect real particle populations. Collectively, the EOS plot confirms the reliability of the zeta-potential measurement, validating that the mobility spectrum is dominated by a single, stable, negatively charged population and supporting the interpretation derived from the primary mobility distribution.

3.8. BET Surface Area Analysis

The peanut shell biochar's nitrogen adsorption–desorption isotherm shows an H3 hysteresis loop and a typical Type IV profile, indicating that mesoporosity produced by the loose stacking of carbonaceous lamellae predominates. Limited micropores are indicated by a minor uptake at low relative pressure ($P/P_0 < 0.1$), but multilayer development within mesoporous domains is shown by the progressive rise in the adsorption branch that follows. In the medium pressure range ($P/P_0 = 0.3–0.4$), the adsorption volume stabilizes around 25–30 $cm^3\ g^{-1}$ STP. The prominent hysteresis loop further suggests the existence of slit-shaped mesopores, which are typical of biochar made from lignocellulosic wastes. The BET

J Water Environ Nanotechnol, 2026, 11(3): 326-344
10.22090/jwent.2025.2073827.1975

Table 5. Experimental parameters for zeta potential measurement of peanut shell–derived biochar.

Parameter	Value	Notes
Upper Surface	-41.14 mV	Surface potential
Lower Surface	-16.65 mV	Surface potential
Diluent Name	WATER	Solvent
Temperature	25.1°C	Measurement condition
Refractive Index	1.3328	Optical property
Cell Type	Flow Cell	Instrument used
Viscosity	0.8858 cP	Fluid property
Avg. Electric Field	-16.63 V/cm	Field strength
Dielectric Constant	78.3	Fluid dielectric property
Avg. Current	-0.11 mA	Measured current

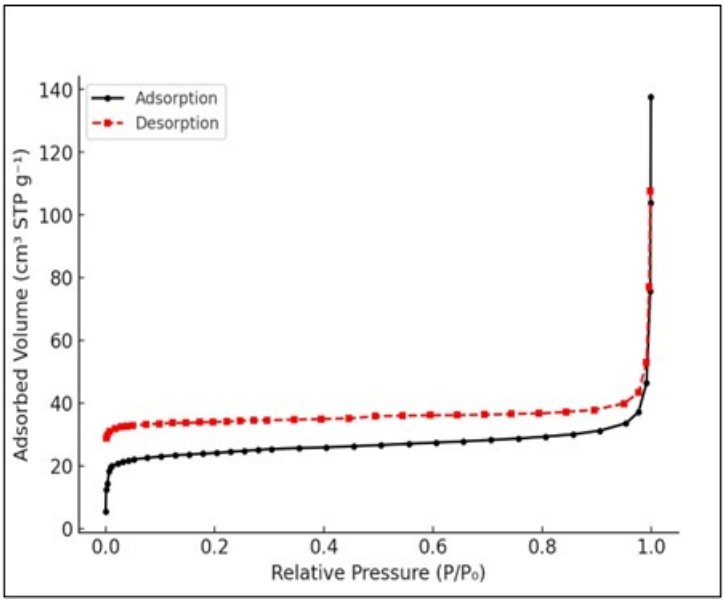

Fig. 11. Nitrogen adsorption–desorption isotherm of peanut shell–derived biochar.

study shows a moderate specific surface area of about 78.6 m^2/g, which is consistent with biochars made at high pyrolysis temperatures but without further activation. Rather than substantial microporosity, a mesoporous structure is confirmed by the mean pore diameter (≈3.69 nm) and total pore volume (≈0.0708 $cm^3\ g^{-1}$). Despite having a moderate surface area, the mesoporous structure greatly enhances functional performance. It improves the ability to store water, makes controlled nutrient release easier, and gives soil microorganisms ideal microhabitats. Additionally, the presence of surface functional groups (–OH, –COOH, –C=O) facilitates metal adsorption, cation exchange, and the stability of organic matter. Overall, the peanut shell biochar's surface and textural qualities show how effective it is as a sustainable soil amendment, enhancing the soil's physicochemical features, nutrient retention, and long-term fertility.

4. EFFECT OF HIGH-TEMPERATURE (800°C) BIOCHAR ON SOIL PHYSICOCHEMICAL PROPERTIES

The inorganic mineral fractions in the biochar made from peanut shells were enhanced by pyrolysis at 800 °C, which encouraged the volatilization of thermally labile organic components. This result is in line with other research showing that greater pyrolysis temperatures promote carbon aromatization, strengthen structural integrity, and increase the mineral content of biochar. In compliance with typical biochar–soil incubation protocols, 2% of the biochar generated at 800 °C was added to the soil.

A clayey soil with a high water-holding capacity, strong nutrient retention, little aeration, and slow drainage—typical of fine-textured, cohesive field sediments—was used in the incubation investigation. At the beginning, this soil had a pH

of 6.5, a cation exchange capacity of 20 cmol kg^{-1}, an organic carbon content of 0.52%, a modest electrical conductivity, and no discernible pollutants. In order to replicate natural oxygen diffusion, both biochar-amended and unamended control soils were incubated for 30 days at 25 ± 2 °C. Moisture levels were maintained at 60% of their water-holding capacity, and aeration was accomplished through gentle mixing every three days.

The physicochemical characteristics of the clayey soil were significantly improved by the addition of the 800 °C biochar under these controlled conditions. Better nutrient retention, increased soil pH, and enhanced moisture stability were made possible by the biochar's greater porosity, increased surface area, and increased cation exchange capacity. In line with previous research, high-temperature biochar increased the availability of important nutrients like potassium, phosphate, and nitrogen while reducing nutrient leaching—a crucial benefit for dense, poorly aerated clay soils.

In conclusion, peanut shell biochar pyrolyzed at 800 °C significantly enhances soil fertility, structural integrity, and nutrient utilization efficiency in clayey soils, highlighting its importance for productivity increases and sustainable soil management [47].

4.1. Mechanistic Reactions and Processes

Ion Exchange and Surface Adsorption

The surface functional groups of biochar interact with nutrient cations (NH_4^+, K^+, Ca^{2+}, Mg^{2+}) through ion exchange and electrostatic attraction, preventing nutrient loss by leaching.

Representative reactions:

$$-COOH + NH_4^+ \rightleftharpoons -COO^- \cdot NH_4^+$$

$$-OH + K^+ \rightleftharpoons -HO^- \cdot K^+$$

These interactions help store nutrients on the biochar matrix, allowing for their gradual release into the rhizosphere.

Microbial Mineralization and Nitrogen Cycling

Biochar provides a favorable microhabitat for soil microorganisms, facilitating the mineralization of organic nitrogen compounds.

Microbial transformation:

$$R\text{–}NH_2 + H_2O \xrightarrow{\text{Microbes}} NH_3 + R\text{–}OH$$

$$NH_3 + H_2O \rightleftharpoons NH_4^+ + OH^-$$

This enhances ammonium (NH_4^+) availability, contributing to improved soil fertility and plant nitrogen uptake.

Phosphate Retention and Controlled Release

PSB adsorbs phosphate anions through surface complexation with hydroxyl groups, ensuring slow and sustained P availability to plants.

Adsorption and release cycle:

$$-OH + H_2PO_4^- \rightleftharpoons -O\text{–}PO_3H_2 + H_2O$$

$$-O\text{–}PO_3H_2 + H_2O \rightarrow -OH + H_2PO_4^-$$

This mechanism mitigates phosphorus fixation and enhances its long-term availability.

Potassium Dissolution from Biochar Matrix

Peanut shells contain inherent potassium oxides (K_2O) and salts that gradually dissolve upon soil contact, releasing K^+ ions for plant uptake.

$$K_2O + H_2O \rightarrow 2K^+ + 2OH^-$$

This process increases soil alkalinity and directly supplies potassium to the root zone.

Carbonate Equilibrium and pH Regulation

The alkaline nature of PSB helps neutralize soil acidity through carbonate and hydroxide formation reactions:

$$CO_2 + H_2O + -OH \rightarrow HCO_3^- + H^+$$

$$Ca^{2+} + 2HCO_3^- \rightarrow CaCO_3 + CO_2 + H_2O$$

The nutrient retention and subsequent release from peanut shell-derived biochar within soil matrices can be schematically represented as follows: The surface of the biochar is characterized by a rich array of functional groups, notably hydroxyl (-OH) and carboxyl (-COOH), which actively facilitate ion exchange processes and the adsorption of crucial nutrients, including ammonium, potassium, calcium, and phosphate. These sequestered nutrients are progressively liberated into the soil through the synergistic actions of microbial mineralization and desorption, thereby augmenting soil fertility, enhancing cation exchange capacity, and optimizing pH levels. Concurrently, this mechanism stimulates microbial activity and effectively mitigates nutrient leaching.

4.2. Soil pH

The observed marginal elevation in pH within soil treated with biochar suggests the inherent alkaline characteristics of biochar. Biochar produced at elevated temperatures typically incorporates basic oxides and carbonates of calcium, potassium, and magnesium, which contribute to the neutralization of soil acidity. This pH modulation fosters an environment more conducive to microbial proliferation and enhances nutrient accessibility [48].

4.3. Electrical Conductivity (EC)

The elevated electrical conductivity observed in biochar-amended soil indicates a greater abundance of soluble ions, including K^+, Ca^{2+}, and Mg^{2+}. This phenomenon is attributed to the liberation of mineral salts from the biochar matrix during the soil incubation process. While augmented electrical conductivity values frequently signify an improved nutrient status, it is crucial to regulate excessive levels to prevent the onset of salinity-related complications [49].

J Water Environ Nanotechnol, 2026, 11(3): 326-344
10.22090/jwent.2025.2073827.1975

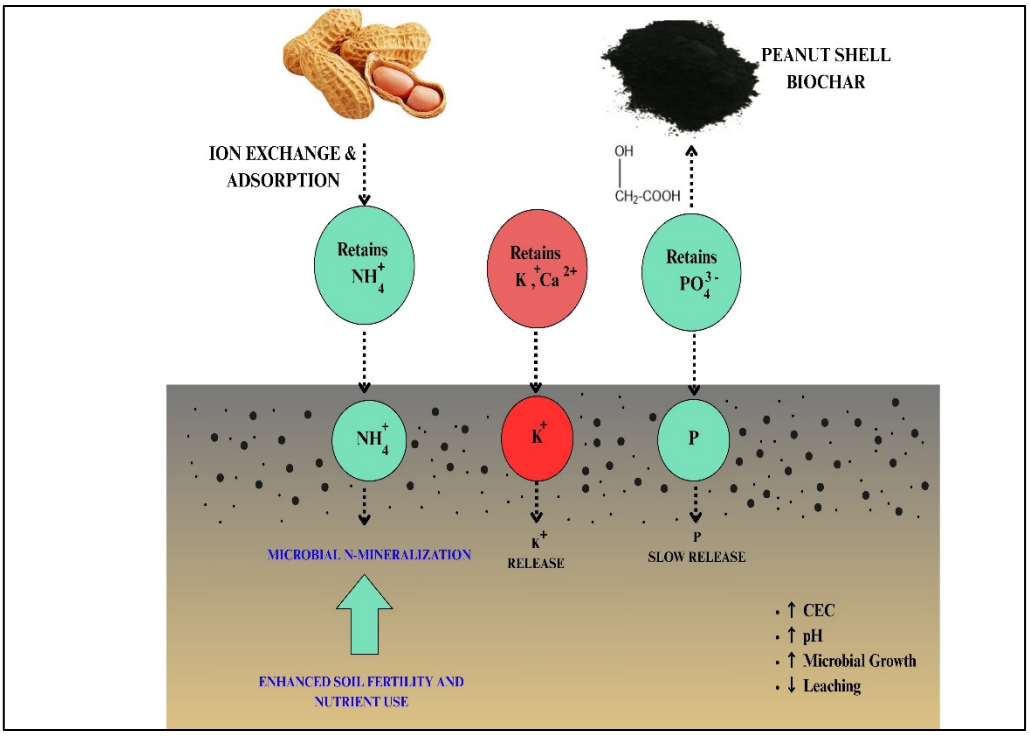

Fig. 12. Mechanism of nutrient retention and release by peanut shell–derived biochar in soil.

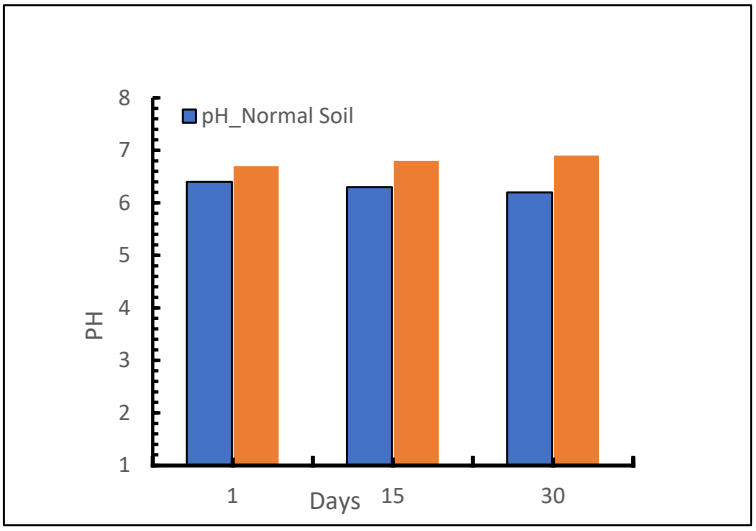

Fig. 13. Variation in soil pH over time in normal and biochar-amended soil.

4.4. Organic Matter Content

A significant increase in organic matter content was observed, indicating that biochar introduces additional carbon and enhances the stability of soil organic carbon. The biochar's highly aromatic and stable carbon structure exhibits resistance to microbial decomposition, consequently improving soil carbon sequestration and fostering better soil texture and aggregation [50].

4.5. Available Nitrogen (N)

The application of biochar to soil resulted in a significant increase in nitrogen concentration, rising from 45 mg/kg to 75 mg/kg over a 30-day interval. This observed augmentation

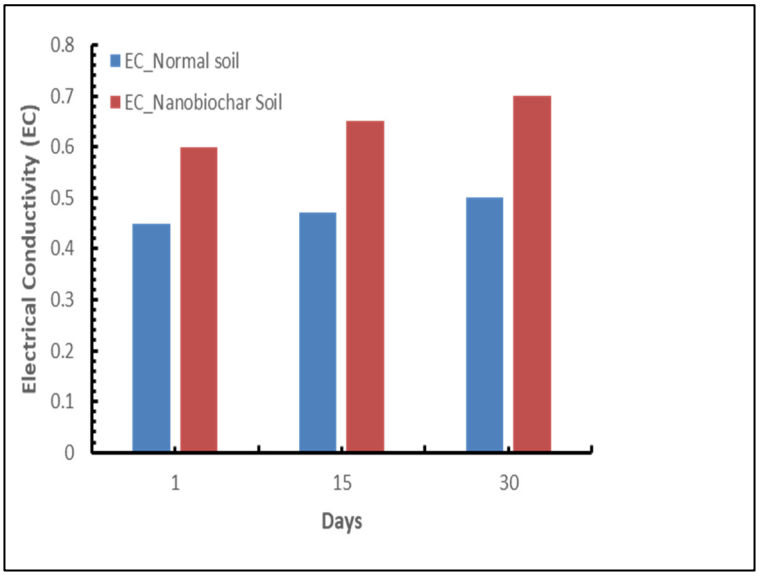

Fig. 14. Electrical conductivity of normal and biochar-amended soil over 30 days.

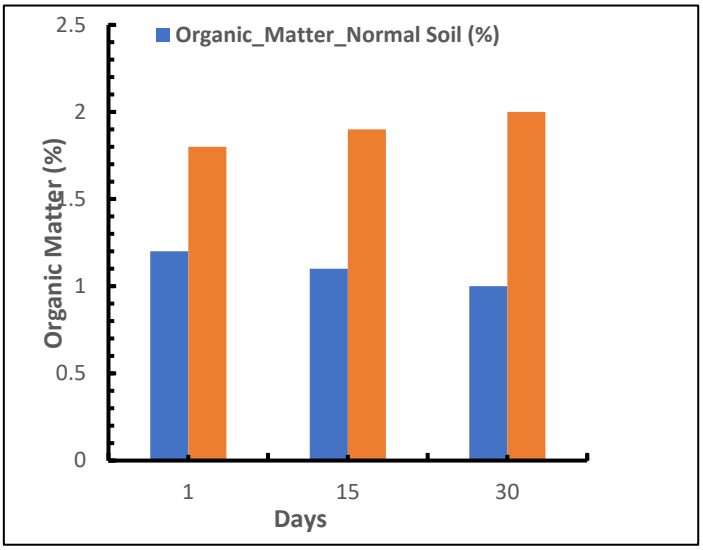

Fig. 15. Organic Matter Content of normal and biochar-amended soil over time

is primarily linked to biochar's high adsorptive capacity, which not only diminishes nitrogen leaching but also stimulates microbial nitrogen fixation. Additionally, the biochar matrix provides a favorable habitat for nitrogen-fixing microorganisms, consequently fostering enhanced nitrogen cycling within the soil [51].

4.6. Available Phosphorus (P)

The concentration of available phosphorus significantly rose from 12 to 24 mg/kg. This increase can be attributed to biochar's surface functional groups and inherent alkalinity, which facilitate the desorption of fixed phosphorus, thereby converting it into more bioavailable forms. Additionally, the elevated temperatures involved in its production lead to an increased ash content, directly enriching the soil system with phosphorus [52].

4.7. Available Potassium (K)

The integration of peanut shell-derived biochar led to a notable elevation in available potassium content, increasing from 90 mg/kg to 130 mg/kg. This enhancement is likely due to the inherent potassium-rich ash residues within biochar generated

J Water Environ Nanotechnol, 2026, 11(3): 326-344
10.22090/jwent.2025.2073827.1975

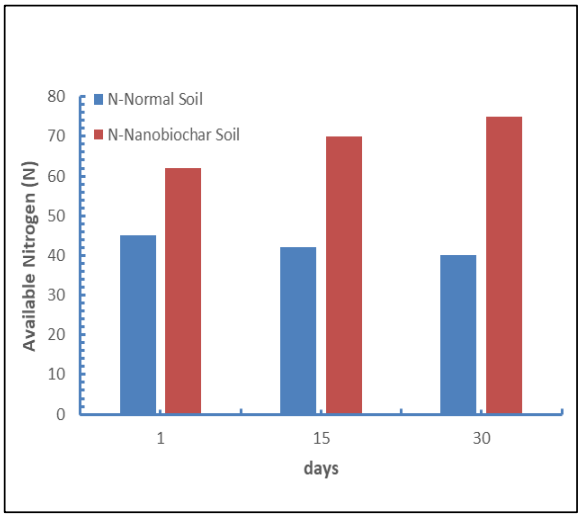

Fig. 16. Available nitrogen in normal and biochar-amended soil over time.

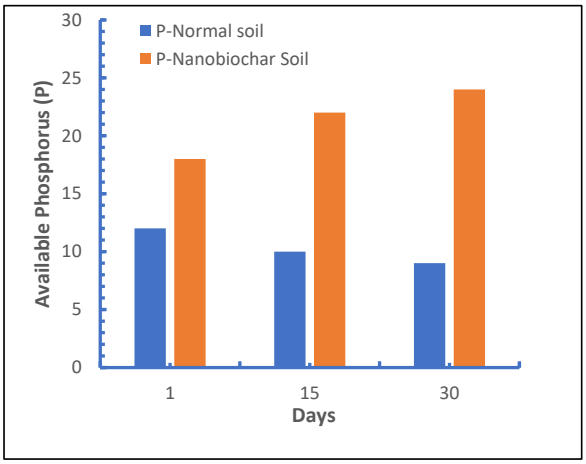

Fig. 17. Available phosphorus in normal and biochar-amended soil over time.

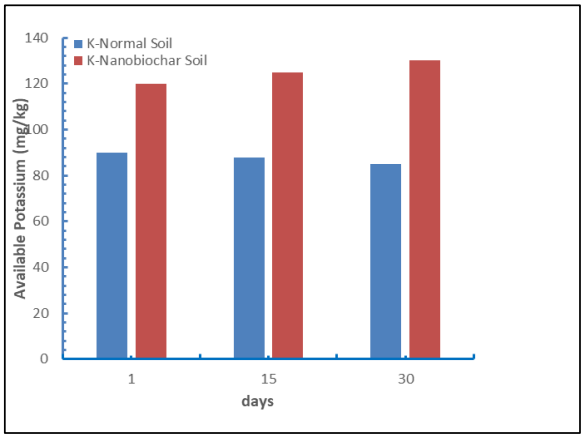

Fig. 18. Available potassium in normal and biochar-amended soil over time.

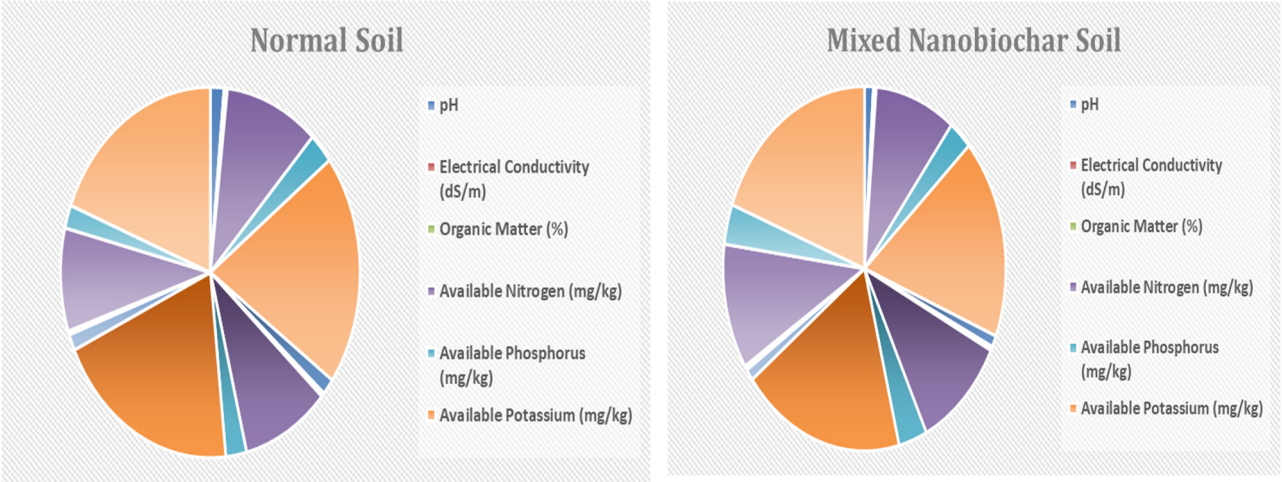

Fig. 19. Comparison of soil properties in normal and biochar-amended soil

Table 6. Effect of Mixed Biochar Amendment on Selected Soil Physicochemical Parameters Over Time

Day	Parameter	Normal Soil	Mixed biochar Soil
1	pH	6.5	6.7
1	Electrical Conductivity (dS/m)	0.45	0.60
1	Organic Matter (%)	1.2	1.8
1	Available Nitrogen (mg/kg)	45	62
1	Available Phosphorus (mg/kg)	12	18
1	Available Potassium (mg/kg)	90	120
15	pH	6.4	6.8
15	Electrical Conductivity (dS/m)	0.47	0.65
15	Organic Matter (%)	1.1	1.9
15	Available Nitrogen (mg/kg)	42	70
15	Available Phosphorus (mg/kg)	10	22
15	Available Potassium (mg/kg)	88	125
30	pH	6.3	6.9
30	Electrical Conductivity (dS/m)	0.50	0.70
30	Organic Matter (%)	1.0	2.0
30	Available Nitrogen (mg/kg)	40	75
30	Available Phosphorus (mg/kg)	9	24
30	Available Potassium (mg/kg)	85	130

from agricultural biomass. Furthermore, the biochar's highly porous architecture promotes a gradual and sustained liberation of K^+ ions, consequently improving nutrient accessibility and plant assimilation over an extended period. This observation aligns with prior research that emphasizes biochar's function in delivering slow-release potassium via mineral dissolution and surface exchange processes [53].

CONCLUSION

This study confirms the efficient conversion of peanut shells into nanostructured biochar through high-temperature pyrolysis at 800 °C, yielding a carbon-rich and thermally stable material with superior physicochemical properties. The resulting nanobiochar exhibits a well-defined mesoporous structure and a predominantly turbostratic carbon framework, along with surface functional groups that enhance nutrient adsorption and retention. When incorporated into soil for 30 days, the biochar produced notable improvements in soil fertility, including increased pH, greater cation exchange capacity, and enhanced availability of nitrogen, phosphorus, and potassium. Its high surface area and reactive pore network facilitated controlled nutrient release, minimized leaching

J Water Environ Nanotechnol, 2026, 11(3): 326-344
10.22090/jwent.2025.2073827.1975

losses, and supported beneficial microbial activity. Overall, peanut shell-derived biochar produced at 800 °C shows strong potential as an effective soil amendment, improving nutrient retention, strengthening soil health, and advancing sustainable agricultural productivity.

Conflict of Interest
The authors declare no conflict of interest.

Funding
This study was not supported by any funding.

Author's Contributions
Study Conception or Design: Deshraj Singh Thakur, Santosh Narayan Chadar
Data Acquisition: Deshraj Singh Thakur
Data Analysis or Interpretation: Deshraj Singh Thakur, Santosh Narayan Chadar
Manuscript Drafting: Deshraj Singh Thakur
Critical Manuscript Revision: Deshraj Singh Thakur
All authors approved the final manuscript and are responsible for all aspects of the work.

AI Statement
The authors confirm that no AI tools or services were used during the preparation of this work.

REFERENCES

1. Holátko J, Elbl J, Kučerík J, Kintl A, Brtnický M. Soil organic carbon: Forms, functions, and management. *Soil Tillage Res.* 2022;221:105418. https://doi.org/10.1016/j.still.2022.105418
2. Lal R. Soil organic matter content and soil quality: The basis of sustainable agriculture. *J Soil Water Conserv.* 2016;71(2):46A–52A. https://doi.org/10.2489/jswc.71.2.46A
3. Chander M, Ghosh S, Sharma DK. Soil organic matter management for sustainable agriculture. *Soil Use Manage.* 2023;39(1):75–86. https://doi.org/10.1111/sum.12884
4. Ray SK, Ghosh S, Mitra B. Soil carbon sequestration and management: A review. *Sustainability.* 2022;14(6):3456. https://doi.org/10.3390/su14063456
5. Singh V, Yadav S, Kumar R. Impact of soil management practices on carbon dynamics in agricultural soils. *Soil Tillage Res.* 2022;218:105320. https://doi.org/10.1016/j.still.2021.105320
6. Bai X, Wang Y, Li C, Wang J. Agricultural waste-derived biochar for environmental applications: Influence of feedstock and pyrolysis conditions. *J Environ Manag.* 2020;256:109926. https://doi.org/10.1016/j.jenvman.2019.109926
7. Zhang X, Gao B, Chen H. Engineered nanobiochar for environmental applications. *Carbon.* 2019;152:401–420. https://doi.org/10.1016/j.carbon.2019.06.026
8. Jat HS, Kumar M, Singh R. Regenerative agricultural practices for enhancing soil organic carbon and resilience. *Agronomy.* 2022;12(5):1147. https://doi.org/10.3390/agronomy12051147
9. Kalikeri S, Yogarajachari RM, Doddananjaiah PH, Gurusiddappa LH, Kachintaya CK. Nano-Enhanced Phytoremediation: Advanced Strategies for Soil Pollutant Remediation and Sustainable Environmental Restoration. *J Water Environ Nanotechnol.* 2025; e725590. https://doi.org/10.22090/jwent.2025.2057480.1914
10. Raiesi Ardali T, Soleimanpour L, Mamani L, Chorom M. Opportunities and Future Perspective of Nanofertilizers and Controlled Release Nanofertilizers in Agriculture. *J Water Environ Nanotechnol.* 2024;9(2):223–47. https://doi.org/10.22090/jwent.2024.02.08
11. Baghaie AH. Organic amendments can affect the heavy metal uptake of the inoculated plant with root-stimulating microorganisms, which was cultivated in contaminated soil. *J Water Environ Nanotechnol.* 2020;5(4):378–87. https://doi.org/10.22090/jwent.2020.04.008
12. Safari Sinegani AA, Noroozi O. Effect of dosage and particle size of natural zeolite on the survival of Escherichia coli in soil. *J Water Environ Nanotechnol.* 2019;4(4):296–307. https://doi.org/10.22090/jwent.2019.04.004
13. Doran JW, Zeiss MR. Soil health and sustainability: Managing the biotic component of soil quality. *Appl Soil Ecol.* 2000;15(1):3–11. https://doi.org/10.1016/S0929-1393(00)00067-6
14. Babu S, Singh R, Kumar S, et al. Biochar implications in cleaner agricultural production and environmental sustainability. *Environ Sci Adv.* 2023;2(8):1042–1059. https://doi.org/10.1039/D2VA00324D
15. Osman M, Elsayed A, Hassan M. Role of biochar in sustainable agriculture: A review. *Agriculture.* 2022;12(9):1375. https://doi.org/10.3390/agriculture12091375
16. Singh Thakur D, Narayan Chadar S. The Role of Nanobiochar in Enhancing Phytoremediation: A New Frontier in Environmental Sustainability. *J Water Environ Nanotechnol.* 2025;10(2):200–26. https://doi.org/10.22090/jwent.2025.02.008
17. Lamrani M, Mouchane M, Taybi H, Mouadili A. Comprehensive Review on the Adsorption Properties of Clay Minerals for Removal of Toxic Dyes and Heavy Metals. *J Water Environ Nanotechnol.* 2025;10(1):85–107. https://doi.org/10.22090/jwent.2025.01.08
18. Fayazi M. Synthesis of ZnO nanostructures with different morphologies on biochar support for photocatalytic degradation of organic dye. *J Water Environ Nanotechnol.* 2024;9(2):137–48. https://doi.org/10.22090/jwent.2024.02.02
19. Duc PA, Hung NV, Van HT. Peanut shell waste valorization for sustainable materials and fuels. *Waste Biomass Valor.* 2019;10(8):2345–2356. https://doi.org/10.1007/s12649-018-0355-7
20. Dantani Meli A, Abdelmonem Abdelfattah M, Nair Gunasegavan RD, Che Abdullah CA. Applying Diverse Plant-Based Methods for Sustainable Synthesis of Titanium Oxide Nanoparticles and Their Environmental Application. *J Water Environ Nanotechnol.* 2025;10(4):417–33. https://doi.org/10.22090/jwent.2025.04.005
21. Mirkazehi Z, Rezaei MR, Sayadi M. Optimization of COD removal of raw landfill leachate using the magnetic graphene oxide/WO3 nanocomposite: isotherms, kinetics, and thermodynamics. *J Water Environ Nanotechnol.* 2023;8(4):320–33. https://doi.org/10.22090/jwent.2023.04.001
22. Puthalapattu RP, Vakati B, Kaveti S, Singh S, Neelam Yugandhar S. Pd@MWCNTs/GCE based voltammetric sensor for butachlor herbicide detection in soil samples. *J Water Environ Nanotechnol.* 2022;7(2):121–31. https://doi.org/10.22090/jwent.2022.02.001
23. Moradi V, Hoodaji M, Kalbasi M. Effect of pyrolysis temperature on peanut shell biochar properties. *J Clean Prod.* 2019;235:342–352. https://doi.org/10.1016/j.jclepro.2019.06.336
24. Ong SK, Chen Z, Singh V. Peanut shell biochar production:

Influence of residence time. *J Anal Appl Pyrolysis.* 2021;158:105276. https://doi.org/10.1016/j.jaap.2021.105276
25. Mukherjee A, Lal R, Zimmerman AR. Biochar impacts on soil physical properties: A review. *Soil Res.* 2022;60(2):153–165. https://doi.org/10.1071/SR21100
26. Abdullah H, Wu H, Gao X. Pyrolysis of biomass and applications in biochar production. *Renew Sust Energ Rev.* 2023;177:113273. https://doi.org/10.1016/j.rser.2023.113273
27. Laird DA, Brown RC, Amonette JE, Lehmann J. Review of the pyrolysis platform for biochar production. *Biofuels Bioprod Bioref.* 2009;3(5):547–562. https://doi.org/10.1002/bbb.169
28. Meyer S, Glaser B, Quicker P. Technical and climate-related aspects of biochar production technologies. *Environ Sci Technol.* 2011;45(22):9473–9483. https://doi.org/10.1021/es201792c
29. Abbhishek A, Kumar R, Singh R. Peanut shell biochar for environmental applications. *Biomass Conv Bioref.* 2021;11(3):1259–1270. https://doi.org/10.1007/s13399-020-00928-5
30. Tongkasee P, Srithat D, Rangsiwiwat A. Phosphate Removal in Tilapia Rearing Effluent by Using CaO Catalyst Synthesized from Moaberry Pomace. *J Water Environ Nanotechnol.* 2025;10(3):285–96. https://doi.org/10.22090/jwent.2025.03.004
31. Pasumarthi R, Venkatesh G, Sharma A. Characterization of peanut shell biochar using pyrolytic kilns. *J Environ Chem Eng.* 2024;12(3):110432. https://doi.org/10.1016/j.jece.2024.110432
32. Sawargaonkar G, Pasumarthi R, Kale S, et al. Valorization of peanut shells through biochar production using slow and fast pyrolysis. *Front Sustain.* 2024;5:1417207. https://doi.org/10.3389/frsus.2024.1417207
33. Qiu T, Li C, Guang M, Zhang Y, Chen J. Porous carbon from microwave-assisted pyrolysis of peanut shells. *Carbon Res.* 2023;2:100079. https://doi.org/10.1007/s44246-023-00079-9
34. Thakur DS, Chadar SN, Lodhi N. Biochar-based nanocomposites: A comparative analysis. *Res Dev Mater Sci.* 2024;21(1):2485–2492. https://doi.org/10.31031/RDMS.2024.21.001003
35. Jones JB. *Laboratory Guide for Conducting Soil Tests and Plant Analysis.* CRC Press; 2001. https://doi.org/10.1201/9781420025293
36. Helmke PA, Sparks DL. Lithium, sodium, potassium, rubidium, and cesium. In: Sparks DL, editor. *Methods of Soil Analysis: Part 3.* Soil Science Society of America; 1996. pp. 551–574. https://doi.org/10.2136/sssabookser5.3.c19
37. Olsen SR, Sommers EL. Phosphorus is soluble in sodium bicarbonate. In: Page AL, editor. *Methods of Soil Analysis: Part 2.* ASA; 1982. pp. 403–430. https://doi.org/10.2134/agronmonogr9.2.2ed.c24
38. Thakur DS, Chadar SN. Coconut shell-based nanobiochar for dye adsorption. *Res Dev Mater Sci.* 2025;14(2):2707–2018. https://doi.org/10.31031/RDMS.2025.22.001034
39. Khater ES, Bahnasawy A, Hamouda R, et al. Biochar production under different pyrolysis temperatures. *Sci Rep.* 2024;14(1):2625. https://doi.org/10.1038/s41598-024-52336-5
40. Goldstein JI, Newbury DE, Joy DC, et al. *Scanning Electron Microscopy and X-ray Microanalysis.* Springer; 2018. https://doi.org/10.1007/978-1-4939-6676-9
41. Liu Z, Dugan B, Masiello CA, et al. Impacts of biochar concentration and particle size on hydraulic properties. *J Hydrol.* 2015;528:576–583. https://doi.org/10.1016/j.jhydrol.2015.06.060
42. Meili L, Cao X, Zhang Y. Mineral phases and surface characteristics of agricultural residue biochar. *J Anal Appl Pyrolysis.* 2019;139:99–107. https://doi.org/10.1016/j.jaap.2019.02.015
43. Liu Z, Zhang FS, Wu J. Biochar from agricultural residues for soil improvement. *Environ Sci Pollut Res.* 2015;22(5):3605–3615. https://doi.org/10.1007/s11356-014-3663-7
44. Sawargaonkar G, Pasumarthi R, Kale S, et al. Valorization of peanut shells using pyrolysis. *Front Sustain.* 2024;5:1417207.
45. He X, Liu Z, Niu W, et al. Effect of pyrolysis temperature on crop residue biochar. *Energy.* 2018;143:746–756. https://doi.org/10.1016/j.energy.2017.11.096
46. Pariyar P, Kumari K, Jain MK, Jadhao PS. Changes in biochar properties with pyrolysis temperature. *Sci Total Environ.* 2020;713:136433. https://doi.org/10.1016/j.scitotenv.2019.136433
47. Paramesh SH, Ananthpur VS, Rajendraprasad N. Natural biodegradable low-cost Lablab purpureus husk as chromatrap for removal of three hazardous organic cationic dyes from water: waste-to-wealth and column elution approach. *J Water Environ Nanotechnol.* 2024;9(1):55–72. https://doi.org/10.22090/jwent.2024.01.04
48. Yuan JH, Xu RK, Zhang H. Forms of alkalis in crop-residue biochar at different temperatures. *Bioresour Technol.* 2011;102(3):3488–3497. https://doi.org/10.1016/j.biortech.2010.11.018
49. Uzoma KC, Inoue M, Andry H, et al. Effect of cow manure biochar on maize under sandy soil. *Soil Use Manage.* 2011;27(2):205–212. https://doi.org/10.1111/j.1475-2743.2011.00340.x
50. Chegeni M, Mehri M, Hosseini M. The MoS2/S-doped graphitic carbon nitride: synthesis and application as a composite for removing organic pollutants. *J Water Environ Nanotechnol.* 2020;5(4):331–41. https://doi.org/10.22090/jwent.2020.04.004
51. Rahmanivahid B, Naderi F, Nayebzadeh H. Removing Methyl Orange Molecules from Aqueous Medium by Magnetic Nanoparticles: Evaluating adsorption factors, isotherms, kinetics, and thermodynamics. *J Water Environ Nanotechnol.* 2020;5(1):1–16. https://doi.org/10.22090/jwent.2020.01.001
52. Liang B, Lehmann J, Solomon D, et al. Black carbon increases cation exchange capacity. *Soil Sci Soc Am J.* 2006;70(5):1719–1730. https://doi.org/10.2136/sssaj2005.0383
53. Deng H, Li G, Yang H, Tang J. Activated carbons from cotton stalk. *Chem Eng J.* 2010;163:373–381. https://doi.org/10.1016/j.cej.2010.08.018